Acta Crystallographica Section C
Crystal Structure Communications
ISSN 0108-2701

Hexakis(urea-κO)zinc(II) dinitrate at 110 and 250 K: uniaxial negative thermal expansion

Stef Smeets and Martin Lutz*

Bijvoet Center for Biomolecular Research, Crystal and Structural Chemistry, Faculty of Science, Utrecht University, Padualaan 8, 3584 CH Utrecht, The Netherlands
Correspondence e-mail: m.lutz@uu.nl

Received 15 December 2010
Accepted 3 January 2011
Online 18 January 2011

The crystal structure of the title compound, $[Zn\{CO(NH_2)_2\}_6](NO_3)_2$, has been determined at 110 and 250 K. The structure is stabilized by 12 individual hydrogen bonds, both intra- and intermolecular. Analysis of the thermal expansion tensor, based on unit cells determined over a temperature range of 180 K, shows uniaxial compression in the direction of the *b* axis during warming. The hydrogen bonds form layers perpendicular to this axis and these layers are connected by coordinative bonds parallel to the axis. As expected, the intermolecular hydrogen bonds expand during warming. Surprisingly, the coordinative bonds contract, accompanied by changes in the O—Zn—O angles. Overall, this behaviour can be described as an accordion-like effect.

Comment

In complex chemistry, urea is a well studied model compound for the coordination of biologically relevant ligands to transition metals *via* the C=O and/or NH_2 groups. According to Mak & Zhou (1992), urea usually acts in metal complexes as a monodentate *O*-bonded ligand, although sometimes the bidentate *N*,*O*-coordination mode is found. Additionally, the Cambridge Structural Database (CSD, August 2010 update; Allen, 2002) contains ten urea complexes showing μ-*O* bridging coordination. In total, the CSD contains 143 urea–transition metal complexes, in 35 of which the metal cation is surrounded by urea as the only ligand.

The structure of hexakis(urea-κO)zinc(II) dinitrate, (I), was determined at room temperature by van de Giesen & Stam (1972). The compound crystallizes in the space group *C*2/*c*, with the Zn^{II} atom on a twofold axis. Zhou *et al.* (1986) described the crystal structure of hexakis(urea-κO)zinc sulfate with cocrystallized solvent water. Prior & Kift (2009) reported the structure of diaquatetrakis(urea-κO)zinc dinitrate, measured at 150 K. We redetermined the structure of (I) at 110 K, (I*a*), and 250 K, (I*b*), in order to obtain more accurate geometries and to determine the thermal expansion behaviour. Unit-cell determinations were performed during cooling from 290 to 110 K and warming from 110 to 250 K, in 20 K intervals.

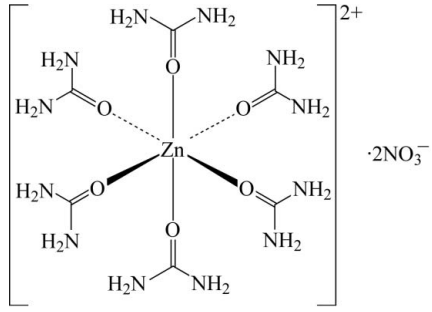

(I)

The overall shape of the cation in (I) is approximately spherical, with a nearly isotropic tensor of inertia. The Zn^{II} atom is surrounded by six urea ligands coordinated by their O atoms (Fig. 1). This is in contrast with urea cadmium nitrate (Catesby, 1961), where the central Cd atom is surrounded by four *O*-coordinated urea ligands. In (I), the ZnO_6 polyhedron has an exact C_2 symmetry and an approximate O_h environment, with r.m.s. deviations of 0.1787 and 0.1307 Å, respec-

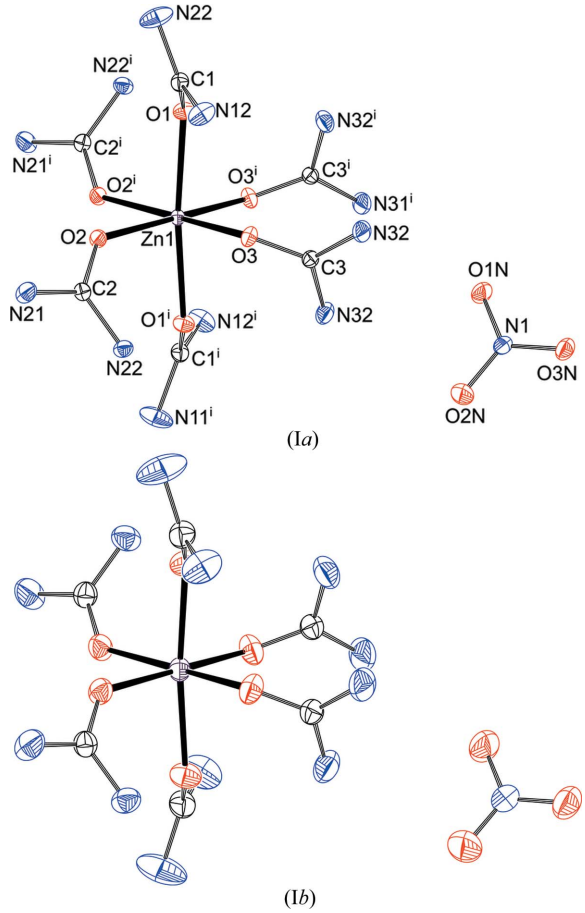

(I*a*)

(I*b*)

Figure 1
Displacement ellipsoid plot and labelling scheme for (I*a*) at 110 K and (I*b*) at 250 K, drawn at the 50% probability level. The labelling scheme is consistent for both figures. H atoms have been omitted for clarity. [Symmetry code: (i) $-x, y, -z+\frac{1}{2}$.]

  doi:10.1107/S0108270111000023

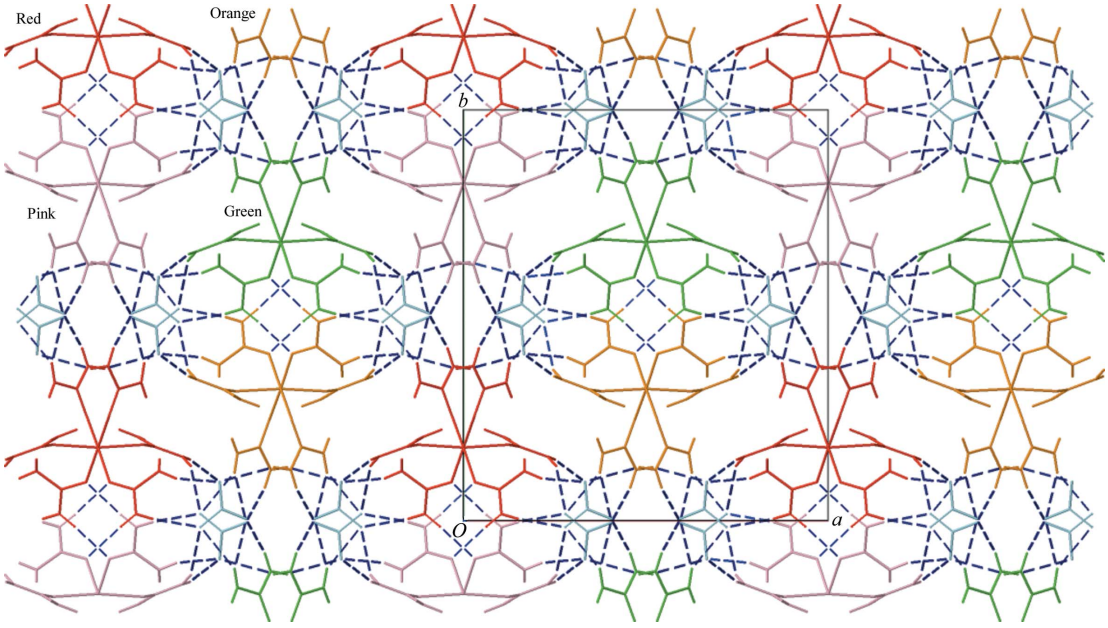

Figure 2
A schematic representation of the hydrogen bonding in (I*a*). Dashed lines indicate intermolecular hydrogen bonds. Each colour represents a different set of symmetry operations, *i.e.* darkest grey (red in the electronic version of the paper): (x, y, z) and ($-x$, y, $-z+\frac{1}{2}$); second-darkest grey (green): ($-x+\frac{1}{2}$, $-y+\frac{1}{2}$, $-z$) and ($x+\frac{1}{2}$, $-y+\frac{1}{2}$, $z-\frac{1}{2}$); second-lightest grey (orange): ($x+\frac{1}{2}$, $y+\frac{1}{2}$, z) and ($-x+\frac{1}{2}$, $y+\frac{1}{2}$, $-z+\frac{1}{2}$); lightest grey (pink): ($-x$, $-y$, $-z$) and (x, $-y$, $z-\frac{1}{2}$). Nitrates are shown in blue. The view is along the crystallographic c axis. (A dynamic version of this figure can be found in the *Supplementary material* for this paper.)

tively, as calculated using the *MOLSYM* program (Pilati & Forni, 1998). The Zn—O1 bond is oriented in the direction of the *a* axis and the Zn—O2 and Zn—O3 bonds are perpendicular to it. The Zn—O1 bond of 2.1366 (6) Å at 110 K is significantly longer than the Zn—O2 and Zn—O3 bonds of 2.0668 (5) and 2.0909 (6) Å, respectively (Tables 1 and 3). The most likely explanation is that atom O1 is an acceptor of two hydrogen bonds, while atoms O2 and O3 accept only one hydrogen bond each. The Zn—O3 bond is slightly longer than Zn—O2, which can be explained by a slightly stronger hydrogen bond with an H···O distance of 2.048 (16) Å, *versus* 2.116 (17) Å at 110 K (Tables 2 and 4). The Zn—O distances are similar to those found in the diaqua complex (Prior & Kift, 2009). There, each urea ligand accepts a single hydrogen bond, resulting in Zn—O_{urea} bond lengths of 2.0893 (15) and 2.0753 (14) Å.

The Zn—O3 bond fails the Hirshfeld rigid-bond test (Hirshfeld, 1976) by 8.50σ at 110 K and 5.50σ at 250 K. The absolute values for the differences are 0.0017 and 0.0022 Å^2 at 110 and 250 K, respectively, which is only slightly larger than the value of 0.0010 Å^2 suggested by Hirshfeld for a rigid bond. We therefore still consider the anisotropic displacement parameters (ADPs) as reliably determined.

The urea ligands are essentially planar, with a maximum deviation of 0.0150 Å from the least-squares planes through their non-H atoms. The planarity at the N atoms has been assessed by evaluating their angle sums. All but one of the N atoms have a planar environment, with angle sums between 355 (2) and 359 (2)° at 110 K. The exception is atom N22, which has an angle sum of 350.0 (19)°, indicating a slight pyramidalization. This is probably due to a close intermolecular contact with atom H12*B*($-x$, y, $-z+\frac{3}{2}$), with an N···H distance of 2.357 (15) Å at 110 K. In the publication of van de Giesen & Stam (1972), this interaction was described as a hydrogen bond. In our opinion, the sp^2-hybridized N atom of urea is not capable of accepting hydrogen bonds, but we still consider this interaction responsible for the slight pyrimidalization, accompanied by a slight elongation of the C—N bond.

During warming from 110 to 250 K, the O3—Zn—O3^{i} angle [symmetry code: (i) $-x$, y, $-z+\frac{1}{2}$] decreases from 97.11 (3) to 96.55 (5)°. This equates to a movement of atom O3 towards the *b* axis. At the same time, the O2—Zn—O2^{i} angle increases from 83.84 (3) to 84.32 (4)°. The O2—Zn—O3 angle stays constant within experimental error [89.58 (2) and 89.62 (3)°].

The crystal packing is stabilized by a hydrogen-bond network consisting of a total of 12 independent hydrogen bonds: three intramolecular N—H···O bonds within the cation (involving atoms H12*A*, H22*A* and H32*A*) and nine intermolecular N—H···O bonds (Tables 2 and 4). The nitrate anion accepts eight of the nine intermolecular hydrogen bonds. Atom H32*B* is involved in a bifurcated hydrogen bond, with atoms O2N and O1N of the nitrate anion as acceptors. All other H atoms are involved in single hydrogen bonds. Atom H12*B* has a short intermolecular contact with atom N22, but we do not consider this as a hydrogen bond (see above). The intermolecular hydrogen bonding results in the formation of layers in the crystallographic *ac* plane (Fig. 2). These layers are interconnected by coordinative bonds from the urea O atoms to the Zn^{II} atoms, and by the intramolecular hydrogen bonds.

To investigate the intermolecular interactions further, temperature-dependent unit-cell determinations were performed by cooling the crystal from 290 to 110 K and then warming from 110 to 250 K, in 20 K intervals. To minimize diffractometer errors in the cell determinations, the *PHI/PHI-*

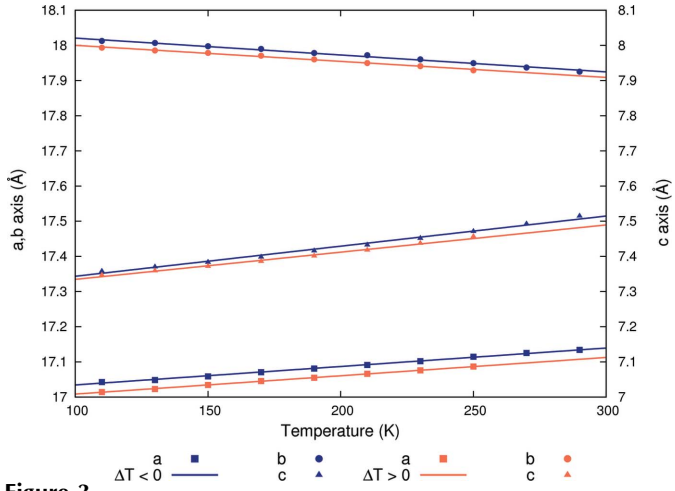

Figure 3
The temperature evolution of the cell parameters (Å) of (I) during cooling from 290 to 110 K (dark-grey lines; blue in the electronic version of the paper) and warming from 110 to 250 K (light-grey lines; red). The scale for the crystallographic *a* and *b* axes is shown on the left, and that for the *c* axis is shown on the right.

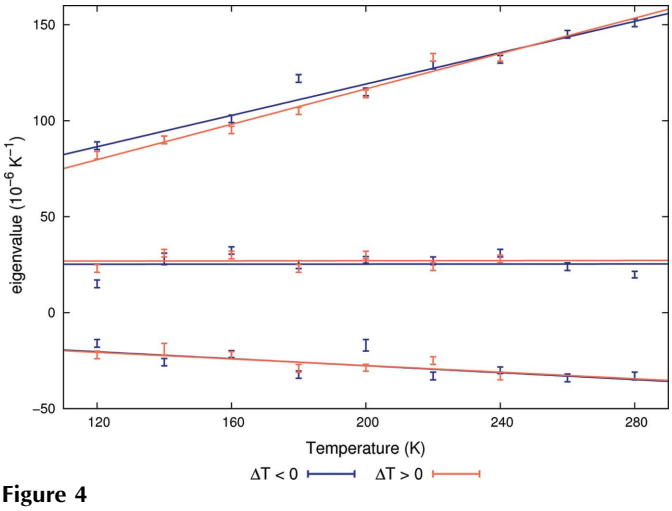

Figure 4
The temperature evolution of the eigenvalues of the unit strain tensor of the thermal expansion (10^{-6} K^{-1}) of (I) during cooling from 290 to 110 K (dark-grey lines; blue in the electronic version of the paper) and warming from 110 to 250 K (light-grey lines; red). Top line: α_1; middle line: α_2; bottom line: α_3.

CHI program was used (Duisenberg *et al.*, 2000) and the position of the detector was kept fixed. The cell axes change linearly with temperature (Fig. 3). The magnitude of the thermal expansion and contraction was assessed by calculation of the expansion tensors using the STRAINANAL routine in *PLATON* (Spek, 2009), which uses the algorithm of Ohashi & Burnham (1973). The thermal expansion tensor is a symmetric second-rank tensor usually expressed in a Cartesian coordinate system (Lovett, 1999). Due to the monoclinic symmetry, two off-diagonal components of the tensor are equal to 0 (Table 5) and one of the eigenvectors (α_3) is parallel to the *b* axis/twofold rotation axis (Table 6). The largest eigenvalues are found for the α_1 direction, which is nearly collinear with the *c* axis. The eigenvalues for the α_2 and α_3 directions have approximately the same magnitude. Interestingly, the eigenvalues for the α_3 direction are negative, as a consequence of a uniaxial compression along the *b* axis during warming (Fig. 4).

Analysis of the thermal expansion tensor can give insight into the strengths of intermolecular interactions (Salud *et al.*, 1998; Küppers, 2003). The largest expansion is expected in the direction of the weakest intermolecular interactions. In (I), the intermolecular hydrogen bonds manifest as two-dimensional layers in the crystallographic *ac* plane. Eigenvalues α_1 and α_2 of the expansion tensor are indeed located in this plane. As expected, the lengths of the intermolecular hydrogen bonds increase during warming. Eigenvalue α_3 is perpendicular to this plane and mainly reflects the interlinkage of the planes *via* coordinative bonds to the Zn atom. This eigenvalue is negative, corresponding to a contraction during warming. Overall, while the layer of hydrogen bonds expands, the distance between the layers decreases, leading to an accordion-like movement. Parallel to the layers, the Zn$\cdots$Zn($\frac{1}{2}-x,\frac{1}{2}-y,-z$) distance increases from 10.6659 (4) Å at 110 K to 10.7358 (4) Å at 250 K. Perpendicular to the layers, the Zn$\cdots$Zn($x,1-y,z+\frac{1}{2}$) distance is shortened from 12.1505 (5) Å at 110 K to 12.1336 (5) Å at 250 K. The combination of the negative eigenvalue of the thermal expansion tensor with the two positive values results in an overall expansion of the unit-cell volume during warming.

Negative thermal expansion is not uncommon in crystals of inorganic compounds. A famous example is the family of cyanide-bridged nanoporous frameworks (Phillips *et al.*, 2008), where transverse vibrations of the cyanide bridges shorten the metal–metal distances. Other framework materials, such as ZrW_2O_8, ZrV_2O_7 and $Sc_2(WO_4)_3$, also show strong negative thermal expansion (Evans, 1999), and a framework-based model has also been used to explain the negative thermal expansion observed in the cuprites Cu_2O and Ag_2O (Artioli *et al.*, 2006). However, in organic compounds, negative thermal expansion is seldom observed. The rigid aromatic molecule pentacene has a very anisotropic molecular shape with an anisotropic tensor of inertia. This can be related to the anisotropy of the libration tensor and the uniaxial negative thermal expansion (Haas *et al.*, 2007). In the monohydrate of the dipeptide tryptophylglycine, the uniaxial negative thermal expansion may be explained by the increased ordering of the solvent water molecule (Birkedal *et al.*, 2002).

Rigid-body analyses were performed on the anisotropic displacement parameters of the cations of (I*a*) and (I*b*) using the program *THMA11* (Schomaker & Trueblood, 1998). In total, 12 rigid-body parameters were refined against 78 independent observations. The weighted *R* values of the resulting **TLS** model are 0.198 at 110 K and 0.173 at 250 K ($R = \{[\Sigma(w\Delta U)^2]/[\Sigma(wU_{obs})^2]\}^{1/2}$, with $w = \langle\sigma\rangle/\sigma$). Such high *R* values indicate significant nonridigity of the complex. This nonrigidity can also be detected by a comparison of the equivalent isotropic displacement parameters [$U_{eq} = \frac{1}{3}\Sigma_{i,j}(U^{ij}a_i^*a_j^*a_ia_j)$]. The U_{eq} values of the N atoms are much larger than those of the other atoms. *PEANUT* plots (Hummel *et al.*, 1990) of the difference between the observed U^{ij} and the U^{ij} from the **TLS** model indicate movement in the out-of-plane directions for the urea ligands (Fig. 5). The largest

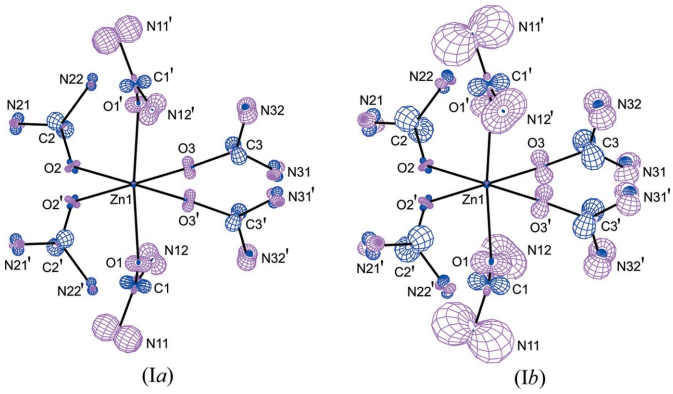

Figure 5
PEANUT plots (Hummel *et al.*, 1990) of the cations of (I*a*) and (I*b*). The plots show the difference between the observed anisotropic displacement parameters (ADPs) and those calculated from a **TLS** model using *THMA11* (Schomaker & Trueblood, 1998). The scale factor is 4.62. Light-grey lines indicate positive differences (purple in the electronic version of the paper) and dark-grey lines negative differences (blue).

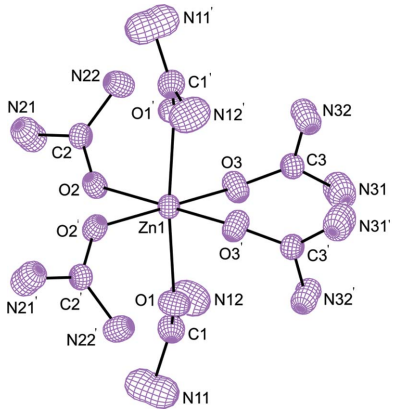

Figure 6
PEANUT plot (Hummel *et al.*, 1990) of the differences between the anisotropic displacement parameters (ADPs) of the cations of (I*a*) and (I*b*), showing r.m.s. surfaces. The atomic coordinates of (I*a*) and its ADPs were transformed to match those of (I*b*) using a quaternion transformation (Mackay, 1984). The scale is 2.31.

differences are observed for urea molecule 1 (atoms O1, C1, N11 and N12) and the smallest for urea molecule 3 (atoms O3, C3, N31 and N32).

The nonrigidity of the cation in (I) can be treated with a segmented rigid-body model, allowing rotations about the O—C bonds. Here, three additional parameters are refined together with the 12 rigid-body parameters. The weighted R values for the **TLS** models improve significantly to 0.138 and 0.126 for (I*a*) at 110 K and (I*b*) at 250 K, respectively. It remains unclear whether this improvement is due to a better model or is simply a consequence of more degrees of freedom. Measurements over more temperatures, together with a normal coordinate analysis (Bürgi & Capelli, 2000), will be necessary for a final judgement on this question.

To analyse further the nonrigidity of the molecule, we looked at the difference between the ADPs of (I*a*) at 110 K and (I*b*) at 250 K. In the first step, the atomic coordinates of (I*a*) were fitted to those of (I*b*) using a quaternion fit (Mackay, 1984). The ADPs of (I*a*) were then transformed accordingly and the difference was visualized using *PEANUT* (Fig. 6). The plot shows the differences in mean-square displacements ($U_{250\ K} - U_{110\ K}$) as a consequence of the temperature increase. It is clearly visible that the nonrigidity of the urea ligands mostly originates from libration around the O—C bond. The largest eigenvectors of the difference ADPs are as good as perpendicular to the urea ligand planes. These directions are different from the *THMA11* result ($U_{calc} - U_{obs}$), which is shown in Fig. 5.

The C, N and O atoms in (I) have rather large anisotropicities, as calculated by the ratio between the highest and lowest eigenvalues (λ_3/λ_1) of the ADPs. They are in the ranges 1.23–4.80 at 110 K and 1.27–5.48 at 250 K. These ratios are larger than in the diaqua compound (Prior & Kift, 2009), which has quite isotropic C, N and O atoms with a maximum (λ_3/λ_1) of 2.85 at 150 K. Restraints on the displacement parameters of two atoms had been used in the refinement of this structure. A redetermination of the structure of the diaqua compound in our laboratory at 150 K gave essentially the same result as that obtained by Prior & Kift (2009), but refinement without restraints on the displacement parameters led to a (λ_3/λ_1) range between 1.40 and 4.07 (Lutz, 2011).

Experimental

Zinc nitrate hexahydrate was mixed with six equivalents of urea in water. Evaporation at room temperature resulted in a highly viscous liquid, from which crystals of (I) were obtained after several weeks.

Data set (I*a*) at 110 K

Crystal data

$[Zn(CH_4N_2O)_6](NO_3)_2$
M_r = 549.76
Monoclinic, $C2/c$
a = 17.0337 (6) Å
b = 18.0092 (5) Å
c = 7.3550 (2) Å
β = 109.651 (2)°
V = 2124.84 (11) Å^3
Z = 4
Mo $K\alpha$ radiation
μ = 1.24 mm^{-1}
T = 110 K
0.36 × 0.20 × 0.12 mm

Data collection

Nonius KappaCCD area-detector diffractometer
Absorption correction: multi-scan (*SADABS*; Sheldrick, 2008*a*)
T_{min} = 0.618, T_{max} = 0.747
40566 measured reflections
4678 independent reflections
4266 reflections with $I > 2\sigma(I)$
R_{int} = 0.027

Refinement

$R[F^2 > 2\sigma(F^2)]$ = 0.022
$wR(F^2)$ = 0.059
S = 1.07
4678 reflections
198 parameters
All H-atom parameters refined
$\Delta\rho_{max}$ = 0.46 e Å^{-3}
$\Delta\rho_{min}$ = −0.27 e Å^{-3}

Data set (I*b*) at 250 K

Crystal data

$[Zn(CH_4N_2O)_6](NO_3)_2$
M_r = 549.76
Monoclinic, $C2/c$
a = 17.1082 (6) Å
b = 17.9456 (7) Å
c = 7.46654 (16) Å
β = 109.701 (2)°
V = 2158.18 (12) Å^3
Z = 4
Mo $K\alpha$ radiation
μ = 1.23 mm^{-1}
T = 250 K
0.36 × 0.20 × 0.12 mm

Table 1
Selected geometric parameters (Å, °) for (I*a*) at 110 K.

Zn1—O1	2.1366 (6)	O1—C1	1.2688 (9)
Zn1—O2	2.0668 (5)	O2—C2	1.2606 (9)
Zn1—O3	2.0909 (6)	O3—C3	1.2642 (9)
O1—Zn1—O1^{i}	173.71 (3)	O2—Zn1—O3	89.58 (2)
O2—Zn1—O2^{i}	83.84 (3)	O2—Zn1—O3^{i}	172.90 (2)
O3—Zn1—O3^{i}	97.11 (3)	C1—O1—Zn1	131.24 (5)
O1—Zn1—O2	93.61 (2)	C2—O2—Zn1	132.76 (5)
O1—Zn1—O3	86.66 (2)	C3—O3—Zn1	127.74 (5)
Zn1—O1—C1—N12	31.21 (11)	Zn1—O2—C2—N22	4.31 (11)
Zn1—O1—C1—N11	−151.71 (7)	Zn1—O3—C3—N31	136.97 (7)
Zn1—O2—C2—N21	−178.34 (6)	Zn1—O3—C3—N32	−46.11 (10)

Symmetry code: (i) $-x, y, -z+\frac{1}{2}$.

Table 2
Hydrogen-bond geometry (Å, °) for (I*a*) at 110 K.

D—H···*A*	*D*—H	H···*A*	*D*···*A*	*D*—H···*A*
N11—H11*A*···O2N^{ii}	0.822 (19)	2.415 (19)	3.1377 (13)	147.3 (17)
N11—H11*B*···O3N^{iii}	0.851 (16)	2.159 (16)	2.9389 (10)	152.1 (14)
N12—H12*A*···O3	0.881 (16)	2.048 (16)	2.8504 (9)	150.9 (14)
N12—H12*B*···N22^{iv}	0.871 (15)	2.357 (15)	3.1705 (10)	155.6 (13)
N21—H21*A*···O2^{v}	0.842 (16)	2.116 (17)	2.9505 (10)	171.0 (15)
N21—H21*B*···O2N^{vi}	0.806 (16)	2.158 (16)	2.9491 (11)	167.1 (15)
N22—H22*A*···O1^{i}	0.833 (14)	2.081 (14)	2.8504 (9)	153.4 (13)
N22—H22*B*···O3N^{vi}	0.828 (14)	2.200 (14)	2.9901 (9)	159.9 (13)
N31—H31*A*···O3N^{vii}	0.823 (16)	2.487 (15)	3.1638 (11)	140.3 (14)
N31—H31*B*···O1N	0.835 (16)	2.220 (16)	2.9820 (11)	151.7 (14)
N32—H32*A*···O1^{i}	0.843 (16)	2.208 (16)	2.9802 (10)	152.4 (14)
N32—H32*B*···O1N	0.868 (15)	2.280 (15)	3.0590 (10)	149.4 (13)
N32—H32*B*···O2N	0.868 (15)	2.553 (15)	3.2089 (11)	133.0 (12)

Symmetry codes: (i) $-x, y, -z+\frac{1}{2}$; (ii) $x-\frac{1}{2}, -y+\frac{1}{2}, z-\frac{1}{2}$; (iii) $x-\frac{1}{2}, y-\frac{1}{2}, z$; (iv) $-x, y, -z+\frac{3}{2}$; (v) $-x, -y, -z+1$; (vi) $-x+\frac{1}{2}, y-\frac{1}{2}, -z+\frac{3}{2}$; (vii) $-x, -y+1, -z+1$.

Data collection

Nonius KappaCCD area-detector diffractometer
Absorption correction: multi-scan (*SADABS*; Sheldrick, 2008*a*)
T_{min} = 0.668, T_{max} = 0.747
41204 measured reflections
4747 independent reflections
4013 reflections with $I > 2\sigma(I)$
R_{int} = 0.030

Refinement

$R[F^2 > 2\sigma(F^2)]$ = 0.029
$wR(F^2)$ = 0.075
S = 1.03
4747 reflections
198 parameters
All H-atom parameters refined
$\Delta\rho_{max}$ = 0.31 e Å^{-3}
$\Delta\rho_{min}$ = −0.44 e Å^{-3}

As a starting model for the refinement, the coordinates of van de Giesen & Stam (1972) were used, but it was decided to perform a unit-cell reduction using *PLATON* (Spek, 2009). Further refinements were performed in the conventional unit-cell setting.

For both data sets, data collection: *COLLECT* (Nonius, 1999); cell refinement: *PEAKREF* (Schreurs, 2008); data reduction: *EVAL15* (Schreurs *et al.*, 2010) and *SADABS* (Sheldrick, 2008*a*); method used to solve structure: coordinates from the literature (van de Giesen & Stam, 1972); program(s) used to refine structure: *SHELXL97* (Sheldrick, 2008*b*); molecular graphics: *PLATON* (Spek, 2009) and *Jmol* (*Jmol*, 2010); software used to prepare material for publication: manual editing of *SHELXL97* CIF file.

Table 3
Selected geometric parameters (Å, °) for (I*b*) at 250 K.

Zn1—O1	2.1428 (8)	O1—C1	1.2633 (12)
Zn1—O2	2.0682 (7)	O2—C2	1.2563 (12)
Zn1—O3	2.0882 (8)	O3—C3	1.2578 (12)
O1—Zn1—O1^{i}	173.81 (5)	O2—Zn1—O3	89.62 (3)
O2—Zn1—O2^{i}	84.32 (4)	O2—Zn1—O3^{i}	173.33 (3)
O3—Zn1—O3^{i}	96.55 (5)	C1—O1—Zn1	131.84 (8)
O1—Zn1—O2	93.61 (3)	C2—O2—Zn1	133.02 (7)
O1—Zn1—O3	86.61 (3)	C3—O3—Zn1	129.29 (7)
Zn1—O1—C1—N12	28.53 (17)	Zn1—O2—C2—N22	4.09 (16)
Zn1—O1—C1—N11	−154.65 (13)	Zn1—O3—C3—N31	137.16 (11)
Zn1—O2—C2—N21	−178.59 (9)	Zn1—O3—C3—N32	−46.38 (16)

Symmetry code: (i) $-x, y, -z+\frac{1}{2}$.

Table 4
Hydrogen-bond geometry (Å, °) for (I*b*) at 250 K.

D—H···*A*	*D*—H	H···*A*	*D*···*A*	*D*—H···*A*
N11—H11*A*···O2N^{ii}	0.80 (3)	2.54 (3)	3.229 (2)	145 (2)
N11—H11*B*···O3N^{iii}	0.84 (2)	2.16 (2)	2.9471 (16)	155 (2)
N12—H12*A*···O3	0.89 (2)	2.06 (2)	2.8722 (14)	150.9 (19)
N12—H12*B*···N22^{iv}	0.860 (19)	2.41 (2)	3.2239 (16)	157.9 (16)
N21—H21*A*···O2^{v}	0.83 (2)	2.14 (2)	2.9671 (14)	171.9 (17)
N21—H21*B*···O2N^{vi}	0.83 (2)	2.14 (2)	2.9605 (17)	166.4 (18)
N22—H22*A*···O1^{i}	0.815 (18)	2.120 (18)	2.8751 (13)	153.9 (16)
N22—H22*B*···O3N^{vi}	0.826 (17)	2.215 (18)	3.0058 (14)	160.1 (15)
N31—H31*A*···O3N^{vii}	0.79 (2)	2.56 (2)	3.2196 (18)	141.2 (18)
N31—H31*B*···O1N	0.79 (2)	2.29 (2)	3.0101 (18)	152.0 (19)
N32—H32*A*···O1^{i}	0.849 (19)	2.239 (19)	3.0078 (15)	150.5 (17)
N32—H32*B*···O1N	0.84 (2)	2.32 (2)	3.0815 (16)	151.5 (17)
N32—H32*B*···O2N	0.84 (2)	2.57 (2)	3.2147 (17)	134.8 (16)

Symmetry codes: (i) $-x, y, -z+\frac{1}{2}$; (ii) $x-\frac{1}{2}, -y+\frac{1}{2}, z-\frac{1}{2}$; (iii) $x-\frac{1}{2}, y-\frac{1}{2}, z$; (iv) $-x, y, -z+\frac{3}{2}$; (v) $-x, -y, -z+1$; (vi) $-x+\frac{1}{2}, y-\frac{1}{2}, -z+\frac{3}{2}$; (vii) $-x, -y+1, -z+1$.

Table 5
Tensor components (10^{-6} K^{-1}) of the unit strain tensor of the thermal expansion for warming from 110 to 250 K.

Tensors are in a Cartesian coordinate system. $\alpha_{12} = \alpha_{23} = 0$, due to symmetry. Orthogonalization matrix: $x//a$, $z//c^*$, $z//y^x$ (Dunitz, 1995).

T (K)	α_{11}	α_{22}	α_{33}	α_{13}
110–130	25.15	−21.76	79.08	−12.08
130–150	33.84	−19.49	86.59	−13.35
150–170	33.11	−22.16	91.61	−14.87
170–190	27.78	−28.89	100.08	−19.81
190–210	32.89	−28.73	110.79	−16.38
210–230	27.96	−24.56	128.82	−20.99
230–250	32.03	−32.78	129.35	−20.36

The authors thank Pascal Parois for his help in applying the quaternion fit to the ADPs (Fig. 6).

Supplementary data for this paper are available from the IUCr electronic archives (Reference: FN3074). Services for accessing these data are described at the back of the journal.

References

Allen, F. H. (2002). *Acta Cryst.* B**58**, 380–388.
Artioli, G., Dapiaggi, M., Fornasini, P., Sanson, A., Rocca, F. & Merli, M. (2006). *J. Phys. Chem. Solids*, **67**, 1918–1922.

Table 6
Eigenvalues of the unit strain tensor of the thermal expansion (10^{-6} K^{-1}) and corresponding angles with the unit-cell axes (°) for warming from 110 to 250 K.

Orthogonalization matrix: $x//a$, $z//c^*$, $z//y^x$ (Dunitz, 1995).

T (K)	Principal axis	Eigenvalue	Angle with a	Angle with b	Angle with c
110–130	α_1	82 (2)	102.1 (13)	90	7.6 (13)
130–150	α_1	90 (2)	103.4 (13)	90	6.2 (13)
150–170	α_1	95.2 (19)	103.5 (12)	90	6.2 (12)
170–190	α_1	105.1 (18)	104.4 (9)	90	5.3 (9)
190–210	α_1	114 (2)	101.4 (6)	90	8.3 (6)
230–250	α_1	133 (2)	101.3 (7)	90	8.3 (7)
110–130	α_2	23 (2)	12.1 (13)	90	97.6 (13)
130–150	α_2	31 (2)	13.4 (13)	90	96.2 (13)
150–170	α_2	30 (2)	13.5 (12)	90	96.2 (12)
170–190	α_2	23 (2)	14.4 (9)	90	95.3 (9)
190–210	α_2	30 (2)	11.4 (6)	90	98.3 (6)
210–230	α_2	24 (2)	11.3 (4)	90	98.4 (4)
230–250	α_2	28 (2)	11.3 (7)	90	98.3 (7)
110–130	α_3	−22 (2)	90	0	90
130–150	α_3	−19 (3)	90	0	90
150–170	α_3	−22.2 (19)	90	0	90
170–190	α_3	−29 (2)	90	0	90
190–210	α_3	−28.7 (18)	90	0	90
210–230	α_3	−25 (2)	90	0	90
230–250	α_3	−33 (2)	90	0	90

Birkedal, H., Schwarzenbach, D. & Pattison, P. (2002). *Angew. Chem. Int. Ed.* **41**, 754–756.
Bürgi, H. B. & Capelli, S. C. (2000). *Acta Cryst.* A**56**, 403–412.
Catesby, C. G. C. (1961). *Nature (London)*, **192**, 254–255.
Duisenberg, A. J. M., Hooft, R. W. W., Schreurs, A. M. M. & Kroon, J. (2000). *J. Appl. Cryst.* **33**, 893–898.
Dunitz, J. D. (1995). *X-ray Analysis and the Structure of Organic Molecules*, 2nd corrected reprint, pp. 235–240. Basel: Verlag Helvetica Chimica Acta.
Evans, J. S. O. (1999). *J. Chem. Soc. Dalton Trans.* pp. 3317–3326.
Giesen, W. van de & Stam, C. H. (1972). *Cryst. Struct. Commun.* **1**, 257–260.
Haas, S., Batlogg, B., Besnard, C., Schilz, M., Kloc, C. & Siegrist, T. (2007). *Phys. Rev. B*, **76**, 205203.
Hirshfeld, F. L. (1976). *Acta Cryst.* A**32**, 239–244.
Hummel, W., Hauser, J. & Bürgi, H.-B. (1990). *J. Mol. Graph.* **8**, 214–220.
Jmol (2010). *Jmol: an open-source Java viewer for chemical structures in three dimensions*. http://www.jmol.org/
Küppers, H. (2003). *International Tables for Crystallography*, Vol. D, edited by A. Authier, pp. 99–104. Dordrecht: Kluwer Academic Publishers.
Lovett, D. R. (1999). *Tensor Properties of Crystals*, 2nd ed. London: IOP Publishing.
Lutz, M. (2011). Private communication (deposition number CCDC 808208). CCDC, Cambridge, England.
Mackay, A. L. (1984). *Acta Cryst.* A**40**, 165–166.
Mak, T. C. W. & Zhou, G.-D. (1992). *Crystallography in Modern Chemistry: A Resource Book of Crystal Structures*, pp. 175–180. Toronto: John Wiley & Sons Inc.
Nonius (1999). *COLLECT*. Nonius BV, Delft, The Netherlands.
Ohashi, Y. & Burnham, C. W. (1973). *Am. Mineral.* **58**, 843–849.
Phillips, A. E., Goodwin, A. L., Halder, G. J., Southon, P. D. & Kepert, C. J. (2008). *Angew. Chem. Int. Ed.* **47**, 1396–1399.
Pilati, T. & Forni, A. (1998). *J. Appl. Cryst.* **31**, 503–504.
Prior, T. J. & Kift, R. L. (2009). *J. Chem. Crystallogr.* **39**, 558–563.
Salud, J., Barrio, M., López, D. O., Tamarit, J. L. & Alcobé, X. (1998). *J. Appl. Cryst.* **31**, 748–757.
Schomaker, V. & Trueblood, K. N. (1998). *Acta Cryst.* B**54**, 507–514.
Schreurs, A. M. M. (2008). *PEAKREF*. University of Utrecht, The Netherlands.
Schreurs, A. M. M., Xian, X. & Kroon-Batenburg, L. M. J. (2010). *J. Appl. Cryst.* **43**, 70–82.
Sheldrick, G. M. (2008*a*). *SADABS*. Version 2008/1. University of Göttingen, Germany.
Sheldrick, G. M. (2008*b*). *Acta Cryst.* A**64**, 112–122.
Spek, A. L. (2009). *Acta Cryst.* D**65**, 148–155.
Zhou, Z., Hu, G., Tang, J., Yu, K., Jiang, G. & Hu, C. (1986). *Huaxue Xuebao (Acta Chim. Sin.)*, **44**, 1045–1048.